



Synthesis, characterization, and photocatalytic activity of co-doped Ag–, Mg–TiO₂-P25 by photodeposition and impregnation methods

Jila Talat-Mehrabad^a, Morteza Khosravi^{a,*}, Nasser Modirshahla^b,
Mohammad A. Behnajady^b

^aDepartment of Applied Chemistry, North Tehran Branch, Islamic Azad University, Tehran, Iran, Tel. +98 914 4198244; email: Jila.talat@gmail.com (J. Talat-Mehrabad), Tel. +98 2122262563; emails: morteza.khosravi22@gmail.com, m_khosravi@iau-tnb.ac.ir (M. Khosravi)

^bDepartment of Chemistry, Tabriz Branch, Islamic Azad University, Tabriz, Iran, Tel. +98 914 1154564; email: Modirshahla@iaut.ac.ir (N. Modirshahla), Tel. +98 9144022644; email: Behnajady@iaut.ac.ir (M.A. Behnajady)

Received 5 October 2014; Accepted 25 March 2015

ABSTRACT

In the present study, Ag–TiO₂-P25 nanoparticle was synthesized using photodeposition technique and Mg was impregnated onto the Ag–TiO₂-P25 for the preparation of co-doped nanoparticles. The physicochemical properties were characterized by X-ray diffraction (XRD), specific surface area and porosity (Brunauer–Emmett–Teller (BET) and Barret–Joyner–Halender), transmission electron microscopy, diffuse reflectance spectroscopy (DRS), scanning electron microscopy, X-ray photoelectron spectroscopy, and energy dispersive X-ray spectroscopy techniques. The BET surface area of the co-doped TiO₂-P25 was larger than that of the monometallic catalysts and the XRD data showed anatase and rutile crystalline phases in catalysts, indicating that Ag and Mg co-doping did not influence the crystal patterns of TiO₂-P25. Also, the DRS results indicated that the band gap of co-doped photocatalyst was smaller than that of the monometallic and undoped TiO₂-P25 and there was a shift in the absorption band toward the visible light region. Additionally, the photocatalytic efficiency of the synthesized catalysts was evaluated by degradation of C.I. Acid Red 27 under visible light irradiation. The results showed that Ag-(1 wt%) and Mg-(0.25 wt %) co-doped TiO₂-P25 had the highest photoactivity among all samples under visible light. The optimum calcination temperature and time were 350 °C and 1 h, respectively. The results of the total organic carbon analysis indicated 66% mineralization of AR27 after 20 min of irradiation time.

Keywords: Heterogeneous photocatalysis; Mg impregnation; Ag photodeposition; TiO₂-P25 nanoparticles; Co-doped; C. I. Acid Red 27

1. Introduction

Heterogeneous photocatalysis has been the most widely used process for photocatalytic degradation of

organic pollutants from aqueous solutions. It is the combination of a semiconductor catalyst (such as TiO₂, CdS, ZnS, ZnO, Fe₂O₃, SrO₂, etc.) and UV or visible light irradiation [1,2]. Compared to other semiconductors, TiO₂ has been regarded as one of the most promising photocatalysts for the photodegradation

*Corresponding author.

process due to its high catalytic efficiency, low cost, stability, nontoxicity, and thermal and electrical properties. Moreover, TiO₂-P25 (Degussa Co) exhibits the highest photocatalytic activity in most of the oxidation reactions compared to various commercially available titania powders. TiO₂-P25 consisting of a mixture of anatase and rutile in a proportion of 80:20% is characterized by a particle size of 21 nm [3,4]. However, its band gap (3.0–3.2 eV) can capture UV light only. One of the most efficient ways to improve photocatalytic activity of TiO₂ is the generation of defects in the lattice through selective metal or nonmetal doping which decreases the band gap energy, and as a result shifts the absorption band to the visible range [5,6]. When TiO₂-P25 is illuminated by photons with an energy level equal to or higher than that of the band gap of the catalyst, electrons are promoted from valence band (VB) to the conduction band (CB) to generate electron–hole pairs on the surface of the catalyst [7,8]. The positive hole and electron are powerful oxidizing and reducing agents, respectively. The comparison between the interfacial charge transfer and the electron–hole pair recombination rate determines photocatalytic properties [9,10]. To reduce electron–hole recombination, several methods have been proposed such as doping and coupling of TiO₂-P25 [11–15]. Based on the findings, co-doping TiO₂ with different elements may lead to better synergistic effects such as N–, S–TiO₂ [16] N–, F–TiO₂ [17] N–, C–TiO₂ [18] and N–, B–TiO₂ [19], monometallic co-doped TiO₂ such as Cu–, S–TiO₂ [20] Ag–, I–TiO₂ [21], and bimetallic co-doped TiO₂ such as Cu–, Ni–TiO₂ [22] Pd–, Ag–TiO₂ [23] Cu–, Ag–TiO₂-P25 [24] and Ni–, Ag–TiO₂ [25]. Other studies have investigated the decomposition of methane over Cu–, Ni–TiO₂ [26] prepared via co-impregnation for photocatalytic reduction of nitrate, Cu–, Zn–TiO₂ [27], Co–, Fe–TiO₂ [28] for rhodamine B degradation, and Cu–TiO₂-P25 for Orange II degradation with 90% color removal in the presence of UVC light [29]. Compared to transition metals and rare earth metals, doping with alkaline earth metals such as Mg and Ca has rarely been reported to date.

In the present study, Ag–TiO₂-P25 nanoparticles were synthesized by photodeposition technique. Both Mg–TiO₂-P25 nanoparticles and bimetallic Ag–, Mg–TiO₂-P25 nanoparticles were prepared by the impregnation method and the catalytic activity of the bimetallic Ag–, Mg–TiO₂-P25 catalyst was compared with its corresponding monometallic Ag–TiO₂-P25, Mg–TiO₂-P25, and TiO₂-P25 catalysts in the degradation of C.I. Acid Red 27 (AR27) from the aqueous solution under visible light. The structural properties of the prepared catalysts were characterized by using

X-ray diffraction (XRD), scanning electron microscopy (SEM), energy dispersive X-ray spectroscopy (EDX), transmission electron microscopy (TEM), X-ray photoelectron spectroscopy (XPS), UV–vis diffuse reflectance spectroscopy (DRS), and specific surface area and porosity (BET and BJH).

2. Experimental

2.1. Materials

Titanium dioxide nanoparticle used in experiments was TiO₂-P25, containing 80% anatase and 20% rutile with a primary particle size of 21 nm, was purchased from Degussa Chemical Company, Germany. Magnesium nitrate hexahydrate and silver nitrate were used as dopant metal salts from Merck Chemical Company, Germany, and AR27, a monoazo anionic dye, was obtained from Merck Co. The chemical structure and other characteristics of AR27 are listed in Table 1.

2.2. Catalyst preparation

2.2.1. Preparation of the Ag–TiO₂-P25 catalyst

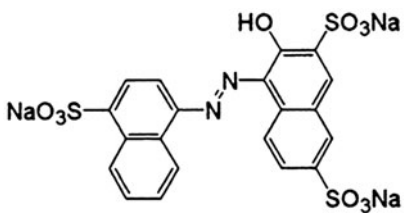
Silver-doped TiO₂-P25 was prepared by photodeposition method. In the first step, 2.72 g TiO₂-P25 was added to 100 mL of deionized water, different concentrations of AgNO₃ (0.2, 0.5, 1, and 1.5 wt%) were then added to TiO₂-P25 suspension for doping. In the second step, the mixture was irradiated with UVC light (15 W, manufactured by Philips, Holland) for 5 h under stirring condition. Afterwards, the precipitate was washed and dried at 80°C for 10 h and calcined in a furnace at 350°C for 3 h.

2.2.2. Preparation of the Mg–TiO₂-P25 and Ag–, Mg–TiO₂-P25 catalysts

For preparation of magnesium-doped TiO₂-P25 nanoparticles, the impregnation method which consisted of the following steps was used: first, an appropriate amount of TiO₂-P25 was added to 30 mL deionized water, and then the required amount of Mg (NO₃)₂·6H₂O for impregnation was added to TiO₂-P25 suspension. Various amounts of Mg (0.15, 0.25, 0.5, and 1 wt%) were used in the preparation of Mg–TiO₂-P25 sample. The obtained titanium suspension was sonicated in an ultrasonic bath (Bandlin EP 2200, 170 W) for 15 min. The suspension was stirred for 4 h at 80°C under reflux conditions, forming a white suspension. By drying the suspension in an oven at 80°C for about 10 h and calcining it at 350°C for 1 h, nano Mg–TiO₂-P25 was prepared. Bimetallic Ag–, Mg–TiO₂-P25

Table 1

Chemical structure and characteristics of C. I. Acid Red 27

Structure	
	
Other names	Amaranth, Azorubin S, FD & C Red 2, C.I. Food Red 9
Molecular formula	C ₂₀ H ₁₁ N ₂ Na ₃ O ₁₀ S ₃
Absorption maximum (λ max)	522 nm
Melting point	120 °C (decomposes)

catalysts were also prepared by the similar procedures and also addition of magnesium nitrate hexahydrate to a calculated amount of Ag–TiO₂-P25 was performed to get the dopant concentration within the range of 0.15–1 wt% and the above procedure was adopted as such.

2.3. Characterization methods

XRD patterns for phase identification and crystallite size calculation were recorded with a Siemens D5000 XRD, using Cu–K α radiation (recorded in the $2\theta = 20\text{--}70^\circ$). The average crystallite size (D in nm) was calculated by Scherrer's equation Eq. (1) [30]:

$$D = k \lambda / \beta \cos \theta \quad (1)$$

where k is a constant equal to 0.89, λ is the X-ray wavelength equal to 0.154056 nm, β is the full width at half maximum intensity, and θ is the half diffraction angle. The phase content of a sample can be calculated from the integrated intensities of anatase (I_A) and rutile (I_R) peaks by the following equation Eq. (2) [31]:

$$\text{Rutile phase \%} = 100 / (1 + 0.8(I_A/I_R)) \quad (2)$$

The DRS of the samples was obtained using the Avaspec-2048 TEC spectrometer to determine the optical band gap (E_g) of catalysts. The band gap energies of all samples were calculated by the following equation Eq. (3):

$$E_g \text{ (eV)} = 1240 / \lambda \text{ (nm)} \quad (3)$$

The chemical composition of the prepared catalysts was analyzed by an EDX system. TEM observation was carried out on Philips CM-10 HT-100 keV electron microscopy instrument. SEM analysis was performed on Au-coated samples using a Philips apparatus model XL30. Nitrogen adsorption–desorption was carried out using Belsorp mini II instrument to measure the specific surface area. The mean pore diameter and total pore volume of the co-doped sample were measured by Brunauer–Emmett–Teller (BET) and Barret–Joyner–Halender (BJH) methods. The surface chemical composition of samples was analyzed by XPS (XPS, twin anode XR3E2 X-ray source). Total organic carbon (TOC) measurements were carried out by TOC analyzer (Shimadzu TOC-V_{csn}).

2.4. Photocatalytic degradation activity of the catalysts

Photocatalytic degradation processes took place in a batch quartz reactor. Visible light irradiation was provided by a 500 W halogen lamp (Osram). In the experiment, 40 mg of photocatalyst was dispersed in 100 mL water for 15 min using an ultrasonic bath (Bandlin EP 2200, 170 W). Then, the desired concentration of AR27 (20 mg L⁻¹) and photocatalyst (40 mg L⁻¹) were fed into the quartz tubular reactor. Prior to irradiation, the solution containing the catalyst was stirred for 30 min in darkness to ensure the establishment of adsorption–desorption equilibrium of AR27 on the catalyst surface. After 30 min, the reaction started when the lamp turned on and 7 mL of the sample was taken out with a Millipore syringe (0.45 μm) at certain time intervals, centrifuged twice for 15 min to remove the suspended solid photocatalyst, and analyzed with a UV–vis spectrophotometer

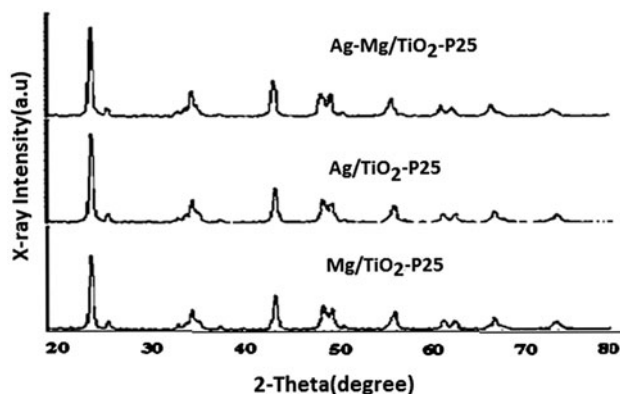


Fig. 1. XRD patterns of Ag-TiO₂-P25 (1 wt%), Mg-TiO₂-P25 (0.25 wt%), and Ag-, Mg-TiO₂-P25 (1-0.25 wt%) calcined at 350°C.

(UV-Shimadzu 2100). The decolorization of AR27 was measured at 522 nm.

3. Results and discussion

3.1. Characterization of the prepared photocatalysts

Fig. 1 shows XRD patterns of Ag-TiO₂-P25 (1 wt%), Mg-TiO₂-P25 (0.25 wt%), and Ag-, Mg-TiO₂-P25 (1-0.25 wt%) calcined at 350°C.

The XRD patterns in the range of 2θ diffraction angle between 20 and 70° were made to obtain the crystallite size and phase composition of nanoparticles (Table 2).

The XRD pattern shown in Fig. 1 mainly consists of an anatase with a minor rutile phase (80: 20), indicating that the Ag and Mg dopants in TiO₂-P25 did not influence the crystal patterns of TiO₂-P25 particle. All the photocatalysts show the dominant anatase phase peaks at $2\theta = 25.2, 38, 48.2, 55, \text{ and } 62.5^\circ$ and the small fraction of the rutile phase with peaks at $2\theta = 27.5, 36, \text{ and } 54^\circ$. Absence of a peak corresponding to silver and magnesium can be due to low doping amount of silver and magnesium content and also proper dispersion of silver and magnesium onto the TiO₂-P25 surface [32].

The TEM image in Fig. 2 shows that the Ag-, Mg-TiO₂-P25 nanoparticles have irregular shape and are agglomerated into larger particles. The size of the Ag-, Mg-TiO₂-P25 nanoparticles corresponds to the crystallite size calculated by the XRD pattern.

The morphology of the Ag- and Mg-co-doped TiO₂-P25 nanoparticles was observed by the SEM technique. Fig. 3 shows the SEM micrograph of the Ag- and Mg-co-doped TiO₂-P25 calcined at 350°C, which indicates a dense structure with fairly good homogeneity. There is an uneven distribution of agglomerated particles. This image shows the particles with a spherical morphology. The SEM micrographs of the sample show that the amounts of Ag- and Mg-co-doped TiO₂-P25 did not influence morphology of the sample.

The chemical composition of the Ag- and Mg-co-doped TiO₂-P25 nanoparticles at the microscopic level was analyzed by EDX. The EDX analysis (Fig. 4(a)) showed that Ti, O, Ag, and Mg peaks were obviously found in the spectra, confirming the presence of both Ag and Mg in the co-doped TiO₂-P25 composition. The mapping spectrum (Fig. 4(b)) of the photocatalysts showed that the dopant metals were well dispersed on TiO₂-P25.

Fig. 5 shows the N₂ adsorption-desorption isotherm of the Ag-TiO₂-P25, Mg-TiO₂-P25, and Ag-, Mg-TiO₂-P25 nanoparticles calcined at 350°C. According to IUPAC classification, Ag-, Mg-TiO₂ nanoparticles display a type-III isotherm and H3 hysteresis, indicating a mesoporous structure. The specific surface areas measured for Ag-TiO₂-P25, Mg-TiO₂-P25, and Ag-, Mg-TiO₂-P25 were 44.3, 45.3, and 46.6 m² g⁻¹, respectively. The pore size distribution of the Ag-, Mg-TiO₂-P25 nanoparticles was obtained from adsorption branch using the BJH method in the range of 34.63 nm. Therefore, the Ag-, Mg-TiO₂-P25 pore structures could be related to the aggregation of TiO₂-P25 crystallites. One of the main problems in the development of TiO₂-P25 was shifting the absorption spectrum of TiO₂-P25 into the visible region to enable more efficient sunlight harvesting. To investigate the effect of magnesium and silver addition on the band gap energy of TiO₂-P25 nanoparticles, DRS was carried out.

Table 2
Phase structure and crystallite size of TiO₂-P25 and doped samples

Catalyst	Calcination temp °C	Crystallite size (nm)	Amount of each phase %	
Ag-TiO ₂ -P25 (1 wt%)	350	DA:18	A:80	R:20
Mg-TiO ₂ -P25 (0.25 wt%)	350	DA:18	A:80	R:20
Ag-, Mg-TiO ₂ -P25 (1-0.25 wt%)	350	DA:18	A:80	R:20

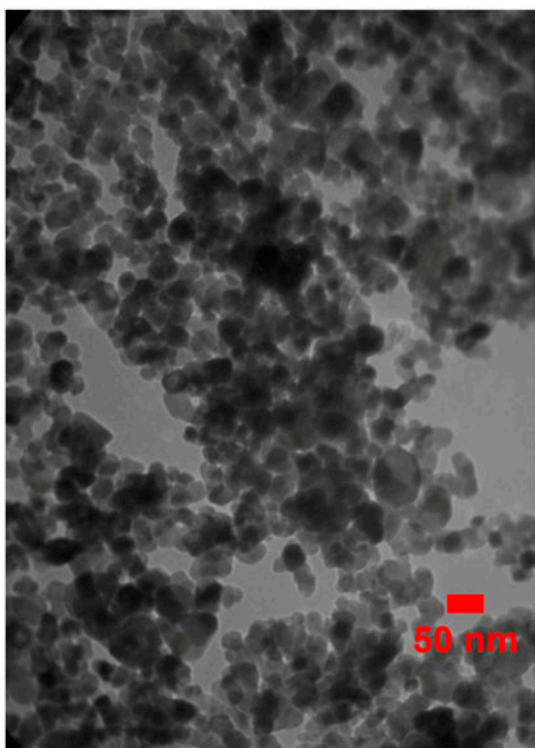


Fig. 2. TEM image of Ag-, Mg-TiO₂-P25 calcined at 350°C.

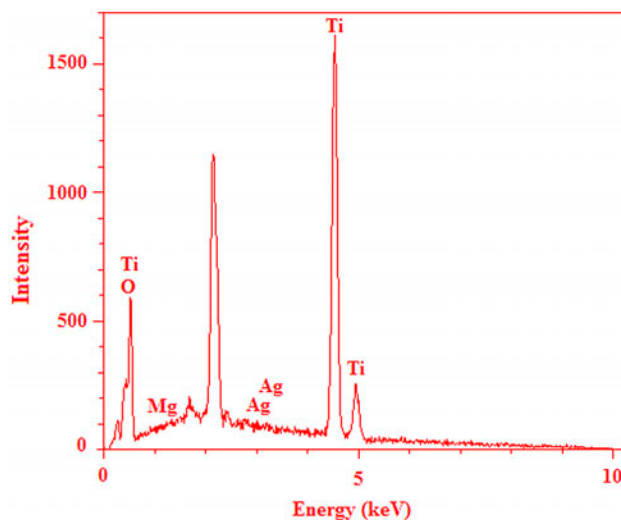


Fig. 4(a). EDX spectrum of Ag-, Mg-TiO₂-P25 nanoparticles.

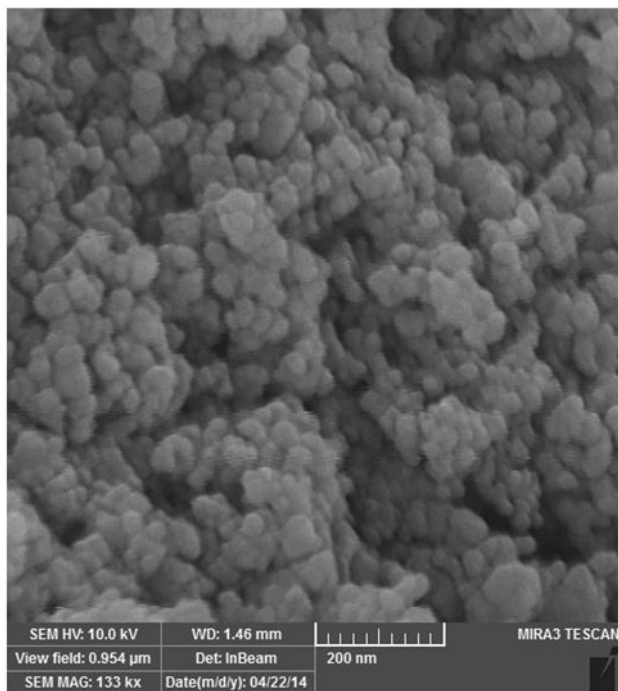


Fig. 3. SEM of Ag-, Mg-TiO₂-P25 calcined at 350°C.

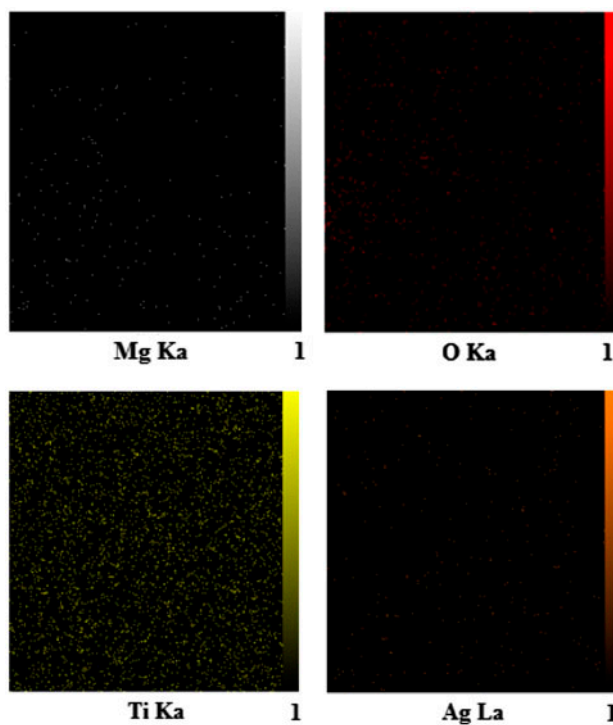


Fig. 4(b). Mapping spectrum of Ag-, Mg-TiO₂-P25 nanoparticles.

Fig. 6 shows the optical absorption of TiO₂-P25, Mg-TiO₂-P25, Ag-TiO₂-P25 and Ag-, Mg-TiO₂-P25 nanoparticles. As mentioned in Fig. 6 and Table 3, the impregnated samples show a long tail extending up to 388, 418, 425, and 434 nm for TiO₂-P25, Mg-TiO₂-P25,

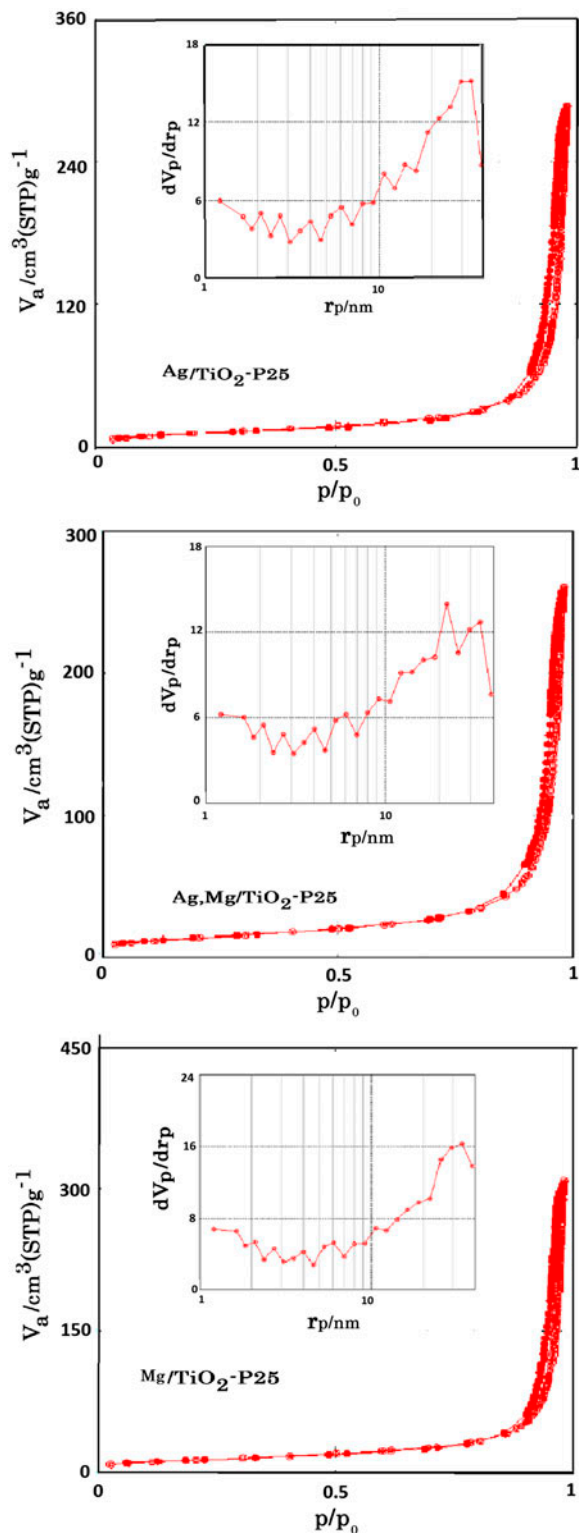


Fig. 5. N₂ adsorption-desorption isotherm of the Ag-TiO₂-P25, Mg-TiO₂-P25, and Ag-, Mg-TiO₂-P25 nanoparticles calcined at 350°C.

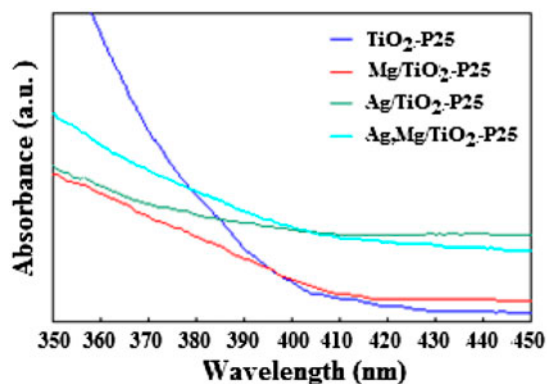


Fig. 6. The DRS-UV-Vis spectra of Degussa P25, Mg-TiO₂-P25, Ag-TiO₂-P25, and Ag-, Mg-TiO₂-P25 nanoparticles.

Table 3

E_g values for monometallic and bimetallic silver- and magnesium-doped TiO₂-P25 nanoparticles

Catalyst	λ_{max} (nm)	E_g (eV)
TiO ₂ -P25	388	3.20
Ag-TiO ₂ -P25	425	2.92
Mg-TiO ₂ -P25	418	2.97
Ag-, Mg-TiO ₂ -P25	434	2.86

Ag-TiO₂-P25, and Ag-, Mg-TiO₂-P25, respectively. The band gap energies of all samples are presented in Table 3. The results indicated that Ag and Mg co-doped onto TiO₂-P25 decreased the optical band gap energy, whereas decrease in E_g value for Ag-, Mg-TiO₂-P25 is greater than that of the monometallic catalysts. This large reduction of band gap may be attributed to the doping of Ag and Mg as impurities into the surface (TiO₂-P25) [33] and production of extra level energy within the band gap; consequently, Fermi energy shifts away from the center of the band gap toward the VB.

XPS analysis of silver- and magnesium-co-doped sample was performed. The survey spectrum and high-resolution scans are shown in Fig. 7. The XPS observations were consistent with EDX results in that only Ag, Mg, Ti, and O elements were detected from the samples in the survey spectrum analysis. Binding energy values for Ag 3d_{5/2} and Ag 3d_{3/2} levels are 367.09 and 373.07 eV, respectively, and the spin energy separation is 6.0 eV, indicating that Ag species exist in their metallic state [34]. The binding energy of Mg 2p was found to be 50.2 eV which is typical of Mg²⁺ [35]. The binding energies of Ti 2p_{3/2} and Ti 2p_{1/2} were found to be 458.3 and 464.012 eV, which are attributed to Ti⁴⁺ [36].

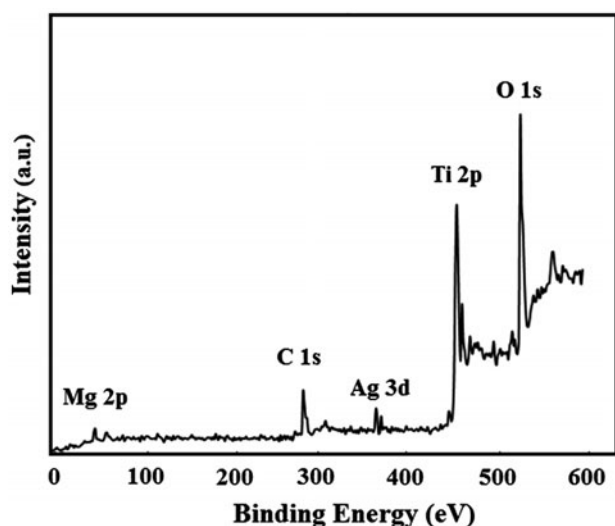


Fig. 7(a). XPS survey spectrum of magnesium- and silver-co-doped TiO₂-P25.

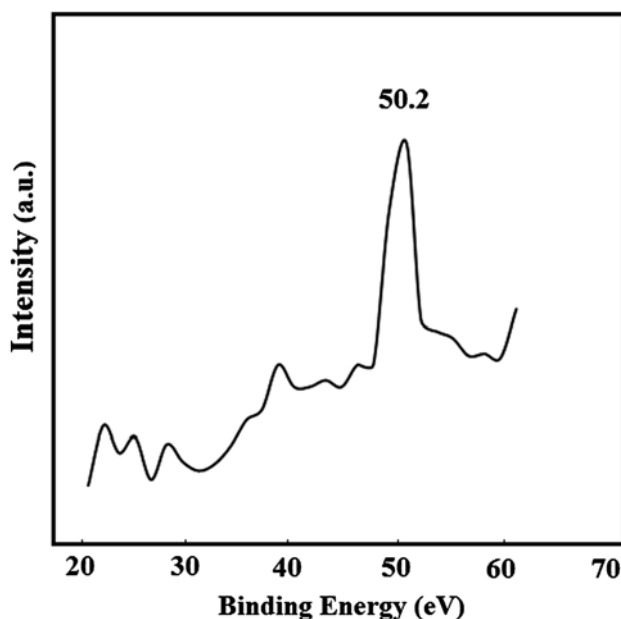


Fig. 7(c). High resolution of Mg 2p spectrum.

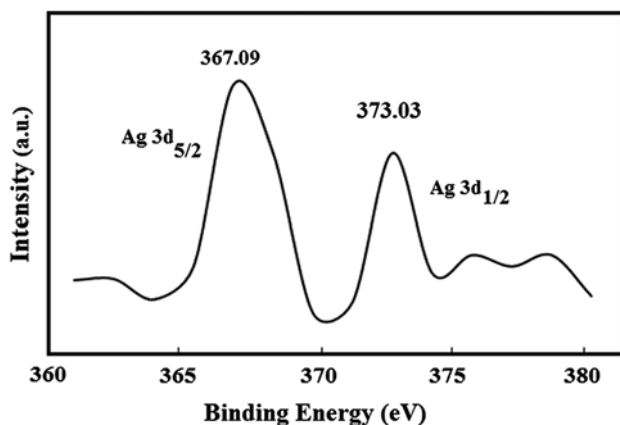


Fig. 7(b). High resolution of Ag 3d spectrum.

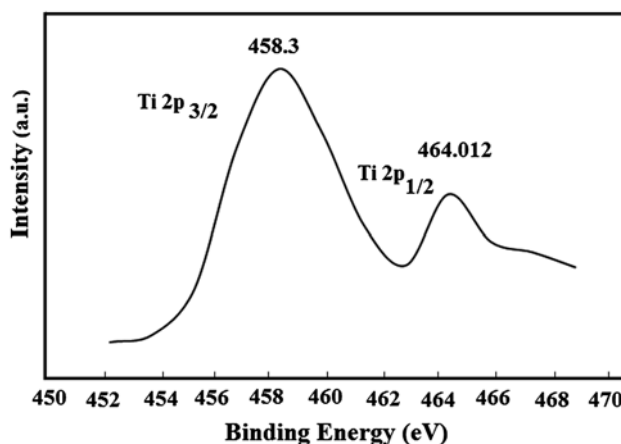


Fig. 7(d). High resolution of Ti 2p spectrum.

3.2. Photocatalytic performance

The photocatalytic oxidation kinetics of many organic compounds have often been modeled on Langmuir–Hinshelwood (L–H), which also cover the adsorption properties of the substrate on the photocatalyst surface [37] as Eq. (4):

$$-d[\text{AR27}]/dt = k_{\text{L-H}}K_{\text{ads}}[\text{AR27}]/(1 + K_{\text{ads}}[\text{AR27}]) \quad (4)$$

where $k_{\text{L-H}}$ is the reaction rate constant ($\text{mg L}^{-1} \text{min}^{-1}$), K_{ads} is the adsorption coefficient of AR27 on the TiO₂-P25 particles ($\text{mg}^{-1} \text{L}$), and [AR27] is the concentration of AR27 (mg L^{-1}). For low concentrations of

AR27 (i.e. $K_{\text{ads}}[\text{AR27}] < 1$), the L–H equation changes into a pseudo-first-order kinetics law as follows Eq. (5):

$$-d[\text{AR27}]/dt = k_{\text{ap}} \times t \quad (5)$$

where $k_{\text{ap}} = k_{\text{L-H}}K_{\text{ads}}$ is the pseudo-first-order rate constant. Integrating Eq. (6), the following equation is obtained Eq. (6):

$$\ln[\text{AR27}]_0/[\text{AR27}] = k_{\text{ap}} \times t \quad (6)$$

Table 4

The apparent reaction rate constant k_{ap} for different catalysts in the photocatalytic degradation of AR27

Catalyst	Metal doping (wt%)		Calcination temp	
	Ag	Mg	°C	k_{ap} (min ⁻¹)
TiO ₂ -P25	0	0	–	0.0380
Mg–TiO ₂ -P25	0	0.25	350	0.0457
Ag–TiO ₂ -P25	0.2	0	350	0.0458
Ag–TiO ₂ -P25	0.5	0	350	0.0521
Ag–TiO ₂ -P25	1	0	350	0.0691
Ag–TiO ₂ -P25	1.5	0	350	0.0492
Ag–, Mg–TiO ₂ -P25	1	0.15	350	0.0941
Ag–, Mg–TiO ₂ -P25	1	0.25	350	0.1279
Ag–, Mg–TiO ₂ -P25	1	0.5	350	0.0781
Ag–, Mg–TiO ₂ -P25	1	0.25	300	0.1005
Ag–, Mg–TiO ₂ -P25	1	1	350	0.0321
Ag–, Mg–TiO ₂ -P25	1	0.25	500	0.0851
Ag–, Mg–TiO ₂ -P25	1	0.25	650	0.0513

where $[AR27]_0$ is the initial concentration of $[AR27]$ (mg L⁻¹) [38].

The semi-logarithmic graphs of the AR27 concentration in the presence of various photo catalysts vs. visible light irradiation time yield straight lines, confirming the pseudo-first-order kinetics for the removal of AR27 in this process. The apparent reaction rate constants (k_{ap}) for the photocatalytic removal of AR27 were obtained from the slope of the semi-logarithmic graphs. Table 4 summarizes the obtained k_{ap} for removal of AR27 in the presence of various Ag–TiO₂-P25, Mg–TiO₂-P25, and Ag–, Mg–TiO₂-P25 nanoparticles. According to these results, k_{ap} increased with Ag loading up to 1 wt% (optimum metal loading), and then decreased. In the photocatalytic process, Ag nanoparticles doped on TiO₂-P25 surface can act as efficient electron–hole separation centers [39,40]. Electron transfer from the CB of TiO₂-P25 to metallic Ag is possible because the Fermi level of silver is lower than that of TiO₂-P25 CB and formation of Schottky barrier is possible in the metallic Ag and TiO₂-P25 contact regions [41,42]. When the number of silver clusters is small, better separation of the electron and hole is achieved. In this process, metallic Ag can promote interfacial charge transfer and inhibit the recombination of photogenerated electron–hole pairs due to its strong electron trap ability, and thus increase the photocatalytic activity. However, in Ag amounts above the optimum value, the Ag nanoparticles can also act as significant recombination centers for photo-generated electron–hole pairs, which results in decreasing the photocatalytic activity of TiO₂-P25 [43]. According to the k_{ap} results presented in Table 4, for Mg impregnation within Ag–TiO₂-P25 nanoparticles,

the highest photocatalytic activity was obtained at the Mg content of 0.25 wt%. This may be attributed to the fact that increased dopant concentration leads to increased number of trapped charge carriers per particle, extending the lifetime of the photogenerated electron–hole pairs. However, an excessive Mg content at the surface of Ag–TiO₂-P25 acts as a significant recombination center for photogenerated electron–hole pairs and inhibits the interfacial electron–hole transfer, leading to a decreased photoactivity [44]. Fig. 8 shows the variations of AR27 k_{ap} in the presence of pure, monometallic, and bimetallic silver- and magnesium-doped TiO₂-P25 nanoparticles. As it is discernible from Fig. 8 and Table 4, bimetallic Ag–, Mg–TiO₂-P25 photocatalyst containing 1 wt% Ag and 0.25 wt% Mg has better photocatalytic activity than Ag–TiO₂-P25, Mg–TiO₂-P25, and TiO₂-P25 in the degradation of

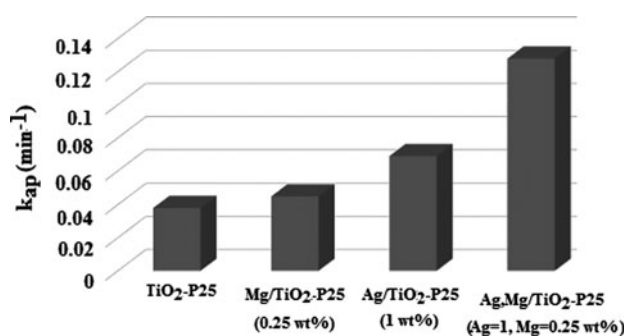


Fig. 8. Comparison between the photocatalytic activity of TiO₂-P25, Mg–TiO₂-P25, Ag–TiO₂-P25, and Ag–, Mg–TiO₂-P25 nanoparticles in the removal of AR27 under visible light irradiation.

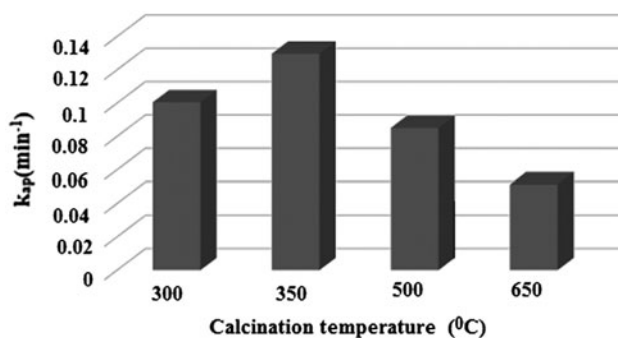


Fig. 9. Effect of calcination temperature on photocatalytic activity of Ag-, Mg-TiO₂-P25 nanoparticles in the removal of AR27 under visible light irradiation.

AR27 because silver and magnesium can separately trap photogenerated electrons and inhibit the recombination of photoinduced electron-hole pairs, and thus improve photocatalytic activity. Furthermore, it can be the highest photocatalytic performance of the co-doped catalyst because of its large surface area. To study the influence of the calcination temperature on the photocatalytic activity of the catalyst, the Ag (1 wt%) and Mg (0.25 wt%) were calcined at 300, 350, 500, and 650 °C for 1 h. As presented in Fig. 9, calcination temperature, which could reach a maximum of 350 °C, had an important effect on the photocatalytic activity of co-doped TiO₂-P25 nanoparticles. It shows that by increasing the calcination temperature, the transformation from rutile to anatase increases while anatase phase has higher photocatalytic activity; thus, photocatalytic activity gradually increases. However, when calcination temperature is above 350 °C, TiO₂-P25 changes from anatase to rutile phase; hence, photocatalytic activity reduces [45]. TOC values are related to the total concentration of organics in the solution and the decrease of TOC reflects the degree of mineralization. The results of TOC showed 66% mineralization of AR27 after 20 min of irradiation in the presence of 400 mg L⁻¹ Ag- and Mg-co-doped TiO₂-P25, whereas 60 min of irradiation was required for complete mineralization (96%).

4. Conclusion

Monometallic and bimetallic TiO₂-P25 nanoparticles impregnated with Ag and Mg were applied to the photocatalytic degradation of AR27. The XRD patterns indicated that adding silver and magnesium to TiO₂-P25 could prevent the phase transformation from anatase to rutile at 350 °C. This is mainly due to the high metal dispersion of the metals onto TiO₂-P25 surface.

The patterns also demonstrated a considerable decrease in E_g value for Ag-, Mg-TiO₂-P25 nanoparticles in comparison with bare and monometallic-doped TiO₂-P25 nanoparticles. The BET results revealed an increase in the surface area of the catalyst, which enhances the photocatalytic degradation of AR27 in visible light. TiO₂-P25 co-doped with 1 wt% Ag and 0.25 wt% Mg displayed the highest photocatalytic activity in the photocatalytic degradation of AR27 compared to monometallic and undoped TiO₂-P25. Such an activity was attributable to the synergistic effects of Ag and Mg co-doping TiO₂-P25. The optimum calcination temperature and time were 350 °C and 1 h, respectively.

Acknowledgment

The authors would like to gratefully acknowledge the support of Islamic Azad University, North Tehran Branch.

List of symbols

k	— constant equal to 0.89
λ	— X-ray wavelength equal to 0.154056 nm
β	— full width at half maximum intensity (FWHM)
θ	— half diffraction angle
I_A	— intensities of anatase peaks
I_R	— intensities of rutile peaks
k_{L-H}	— reaction rate constant (mg L ⁻¹ min ⁻¹)
K_{ads}	— adsorption coefficient of AR27 on the TiO ₂ -P25 particles (mg ⁻¹ L)

References

- [1] M.A. Behnajady, H. Eskandarloo, N. Modirshahla, M. Shokri, Influence of the chemical structure of organic pollutants on photocatalytic activity of TiO₂ nanoparticles: Kinetic analysis and evaluation of electrical energy per order (E_{EO}), Dig. J. Nanomater. Bios. 6 (2011) 1887–1895.
- [2] S. Chakrabarti, B.K. Dutta, Photocatalytic degradation of model textile dyes in wastewater using ZnO as a semiconductor catalyst, J. Hazard. Mater. 112 (2004) 269–278.
- [3] M.A. Behnajady, B. Alizade, Enhancement of TiO₂-UV100 nanoparticles photocatalytic activity by Mg impregnation in the removal of a model organic pollutant, Desalin. Water Treat. 53 (2015) 689–696.
- [4] J. Arana, J.M. Dona Rodriguez, D. Portillo Carrizo, C. Fernandez Rodriguez, J. Perez Pena, O. Gonzalez Diaz, J.A. Navio, M. Macias, Photocatalytic degradation of phenolic compounds with new TiO₂ catalysts, Appl. Catal. B 100 (2010) 346–354.

- [5] M.R. Hoffmann, S.T. Martin, W.Y. Choi, D.W. Bahnemann, Environmental applications of semiconductor photocatalysis, *Chem. Rev.* 95 (1995) 69–96.
- [6] A.V. Emeline, G.V. Kataeva, V.K. Ryabchuk, N. Serpone, Photostimulated generation of defects and surface reactions on a series of wide band gap metal-oxide solids, *J. Phys. Chem. B* 103 (1999) 9190–9199.
- [7] M.A. Behnajady, S. Ghorbanzadeh Moghaddam, N. Modirshahla, M. Shokri, Investigation of the effect of heat attachment method parameters at photocatalytic activity of immobilized ZnO nanoparticles on glass plate, *Desalination* 249 (2009) 1371–1376.
- [8] Z. Wang, W. Ma, C. Chen, H. Ji, J. Zhao, Probing paramagnetic species in titania based heterogeneous photocatalysis by electron spin resonance (ESR) spectroscopy, *Chem. Eng. J.* 170 (2011) 353–362.
- [9] M.A. Behnajady, B. Alizade, N. Modirshahla, Synthesis of Mg-doped TiO₂ nanoparticles under different conditions and its photocatalytic activity, *Photochem. Photobiol.* 87 (2011) 1308–1314.
- [10] L. Gomathi Devi, N. Kottam, B. Narasimha Murthy, S. Girish Kumar, Enhanced photocatalytic activity of transition metal ions Mn²⁺, Ni²⁺ and Zn²⁺ doped polycrystalline titania for the degradation of Aniline Blue under UV/ solar light, *J. Mol. Catal. A: Chem.* 328 (2010) 44–52.
- [11] D. Li, H. Haneda, S. Hishita, N. Ohashi, Visible-light-driven N-F-codoped TiO₂ photocatalysts. 1. Synthesis by spray pyrolysis and surface characterization, *Chem. Mater.* 17 (2005) 2588–2595.
- [12] W.F. Yao, H. Wang, X.H. Xu, X.N. Yang, Y. Zhang, S.X. Shang, M. Wang, Preparation and photocatalytic property of La (Fe)-doped bismuth titanate, *Appl. Catal. A* 251 (2003) 235–239.
- [13] D. Li, H. Haneda, S. Hishita, N. Ohashi, Visible-light-driven N-F-codoped TiO₂ photocatalysts. 2. Optical characterization, photocatalysis, and potential application to air purification, *Chem. Mater.* 17 (2005) 2596–2602.
- [14] D. Li, N. Ohashi, S. Hishita, T. Kolodiazhnyi, H. Haneda, Origin of visible-light driven photocatalysis: A comparative study on N/F-doped and N-F-codoped TiO₂ powders by means of experimental characterizations and theoretical calculations, *J. Solid State Chem.* 178 (2005) 3293–3302.
- [15] K. Song, J. Zhou, J. Bao, Y. Feng, Photocatalytic activity of (copper, nitrogen)-codoped titanium dioxide nanoparticles, *J. Am. Ceram. Soc.* 91 (2008) 1369–1371.
- [16] F.Y. Wei, L.G. Ni, P. Cui, Preparation and characterization of N-S-codoped TiO₂ photocatalyst and its photocatalytic activity, *J. Hazard. Mater.* 156 (2008) 135–140.
- [17] G. Yang, T. Wang, B. Yang, Z. Yan, S. Ding, Enhanced visible-light activity of F-N codoped TiO₂ nanocrystal via nonmetal impurity, Ti³⁺ ions and oxygen vacancies, *Appl. Surf. Sci.* 287 (2013) 135–142.
- [18] K.R. Wu, C.W. Yeh, C.H. Hung, C.Y. Chung, L.H. Cheng, Photoelectrochemical properties of N/C-codoped TiO₂ film electrodes prepared by reactive DC magnetron sputtering, *J. Nanosci. Nanotechnol.* 10 (2010) 1057–1064.
- [19] N.O. Gopal, H.H. Lo, S.C. Ke, Effect of nitrogen-doping temperature on the structure and photocatalytic activity of the B, N-doped TiO₂, *J. Am. Chem. Soc.* 130 (2008) 2760–2765.
- [20] M. Hamadani, A. ReisiVanani, A. Majedi, Synthesis, characterization and effect of calcination temperature on phase transformation and photocatalytic activity of Cu, S-codoped TiO₂ nanoparticles, *Appl. Surf. Sci.* 256 (2010) 1837–1844.
- [21] L. Liao, C.W. Ingram, Mesoporous I-Ag codoped titania and alumina modified titania catalysts: Synthesis, characterization and photocatalytic properties, *Appl. Catal. A* 433–434 (2012) 18–25.
- [22] N. Riaz, F.K. Chong, B.K. Dutta, Z.B. Man, M.S. Khan, E. Nurlaela, Photodegradation of Orange II under visible light using Cu–Ni/TiO₂: Effect of calcination temperature, *Chem. Eng. J.* 185–186 (2012) 108–119.
- [23] K. Kontapakdee, J. Panpranot, P. Praserttham, Effect of Ag addition on the properties of Pd–Ag/TiO₂ catalysts containing different TiO₂ crystalline phases, *J. Catal.* 8 (2007) 2166–2170.
- [24] M.A. Behnajady, H. Eskandarloo, Silver and copper co-impregnated onto TiO₂-P25 nanoparticles and its photocatalytic activity, *Chem. Eng. J.* 228 (2013) 1207–1213.
- [25] H.Y. Chuang, D.H. Chen, Fabrication and photocatalytic activities in visible and UV light regions of Ag@TiO₂ and NiAg@TiO₂ nanoparticles, *J. Nanotechnol.* 20 (2009) 105704–105714.
- [26] W. Gao, R. Jin, J. Chen, X. Guan, H. Zeng, F. Zhang, N. Guan, Titania-supported bimetallic catalysts for photocatalytic reduction of nitrate, *Catal. Today* 90 (2004) 331–336.
- [27] D. Zhang, F. Zeng, Photocatalytic oxidation of organic dyes with visible-light driven codoped TiO₂ photocatalysts, *J. Phys. Chem. A* 85 (2011) 1077–1083.
- [28] W. Zhuyi, C. Chen, F. Wu, B. Zou, M. Zhao, J. Wang, C. Feng, Photodegradation of rhodamine B under visible light by bimetal codoped TiO₂ nanocrystals, *J. Hazard. Mater.* 2 (2009) 615–620.
- [29] R.S.K. Wong, J. Feng, X. Hu, P.L. Yue, Discoloration and mineralization of nonbiodegradable azo dye Orange II by copper-doped TiO₂ nanocatalysts, *J. Environ. Sci. Health. Part A* 39 (2005) 2583–2595.
- [30] A.L. Patterson, The scherrer formula for X-Ray particle size determination, *J. Phys. Rev.* 56 (1939) 978–982.
- [31] R.A. Spurr, H. Myers, Quantitative analysis of anatase-rutile mixtures with an X-Ray diffractometer, *J. Anal. Chem.* 29 (1957) 760–762.
- [32] Y. Li, S. Peng, F. Jiang, G. Lu, S. Li, Effect of doping TiO₂ with alkaline-earth metal ions on its photocatalytic activity, *J. Serb. Chem. Soc.* 72 (2007) 393–402.
- [33] Q. Wang, S. Xu, F. Shen, Preparation and characterization of TiO₂ photocatalysts co-doped with iron (III) and lanthanum for the degradation of organic pollutants, *Appl. Surf. Sci.* 257 (2011) 7671–7677.
- [34] L. Sun, J. Li, C. Wang, S. Li, Y. Lai, H. Chen, C. Lin, Ultrasound aided photochemical synthesis of Ag loaded TiO₂ nanotube arrays to enhance photocatalytic activity, *J. Hazard. Mater.* 171 (2009) 1045–1050.
- [35] J.S. Corneille, J. Wei He, D. Wayne Goodman, XPS characterization of ultra-thin MgO films on a Mo (100), *Surf. Sci.* 306 (1994) 269–278.
- [36] S.S. Mandal, A.J. Bhattacharyya, Electrochemical sensing and photocatalysis using Ag–TiO₂ microwires, *J. Chem. Sci.* 124 (2012) 969–978.

- [37] C.S. Turchi, D.F. Ollis, Photocatalytic degradation of organic water contaminants: Mechanisms involving hydroxyl radical attack, *J. Catal.* 122 (1990) 178–192.
- [38] M.A. Behnajady, N. Modirshahla, R. Hamzavi, Kinetic study on photocatalytic degradation of C.I. Acid Yellow 23 by ZnO photocatalyst, *J. Hazard. Mater.* 133 (2006) 226–232.
- [39] R. Georgekutty, M.K. Seery, S.C. Pillai, A highly efficient Ag-ZnO photocatalyst: Synthesis, Properties, and mechanism, *J. Phys. Chem. C* 112 (2008) 13563–13570.
- [40] H.M. Coleman, K. Chiang, R. Amal, Effects of Ag and Pt on photocatalytic degradation of endocrine disrupting chemicals in water, *Chem. Eng. J.* 113 (2005) 65–72.
- [41] M.K. Seery, R. George, P. Floris, S.C. Pillai, Silver doped titanium dioxide nanomaterials for enhanced visible light photocatalysis, *J. Photochem. Photobiol. A* 189 (2007) 258–263.
- [42] M.S. Lee, S.S. Hong, M. Mohseni, Synthesis of photocatalytic nanosized TiO₂-Ag particles with sol-gel method using reduction agent, *J. Mol. Catal. A: Chem.* 242 (2005) 135–140.
- [43] Y. Cao, H. Tan, T. Shi, T. Tang, J. Li, Preparation of Ag-doped TiO₂ nanoparticles for photocatalytic degradation of acetamiprid in water, *J. Chem. Technol. Biotechnol.* 83 (2008) 546–552.
- [44] S. Ahmed, M.G. Rasul, W.N. Martens, R. Brown, M.A. Hashib, Heterogeneous photocatalytic degradation of phenols in wastewater: A review on current status and developments, *Desalination* 26 (2010) 3–18.
- [45] M.A. Behnajady, H. Eskandarloo, Characterization and photocatalytic activity of Ag-Cu/TiO₂ nanoparticles prepared by sol-gel method, *J. Nanosci. Nanotechnol.* 13(1) (2013) 548–553.